

THE DESIGN OF DRILLED DISPLACEMENT SYSTEM PILES USING THE CAVITY EXPANSION THEORY

NAČRTOVANJE SISTEMA UVRTANIH PILOTOV Z ODMIKANJEM Z UPORABO TEORIJE RAZŠIRJANJA PROSTORA

Stacho Jakub

Slovak University of Technology in Bratislava,
Faculty of Civil Engineering
Radlinskeho 11, 810 05 Bratislava, Slovakia
E-mail: jakubstacho22@gmail.com

DOI <https://doi.org/10.18690/actageotechslov.15.2.81-91.2018>

Keywords

pile foundation, drilled displacement system pile, cavity expansion theory, static load test

Ključne besede

temeljenje na pilotih, sistem uvrtnih pilotov z odmikanjem, teorija razširjanja prostora, statični obremenilni preizkus

Abstract

Drilled Displacement System (DDS) piles are an innovative technology for pile foundations. These DDS piles are created by rotary drilling with a simultaneous full displacement of the soil in a horizontal direction. The optimal design of DDS piles can be obtained in sandy soils and fine-grained soils that allow for a horizontal displacement, which causes an increase in the shaft's resistance. This article deals with the use of Cavity Expansion Theory (CET) for a complex analysis of DDS piles. This method makes it possible to take into account the impact of the technology in pile design. A general view of the CET is presented and is described step by step for the solution of the present problem. The results of the calculations are compared and analysed with the results of three instrumented static load tests. The analyses include a comparison of the load-settlement curve as well as the load distribution over the pile's length, which was measured using strain gauges. The results of the analyses show very good agreement between the calculations and the measurements. The difference between the calculated and measured load-settlement curves did not exceed a 10% degree of accuracy. The possibilities for the future use of CET are also discussed.

Izvleček

Uvrtni piloti z odmikanjem (DDS) predstavljajo inovativno tehnologijo za temeljenje pilotov. Pilote izvedemo po tehnologiji DDS z rotacijskim vrtnjem in hkratnim polnim odmikanjem tal v vodoravni smeri. Optimalno obliko DDS pilotov lahko dobimo v peščenih in drobnozrnatih zemljinah, ki omogočajo vodoravno odmikanje, kar povzroči povečanje nosilnosti pilota na plašču. Ta članek obravnava uporabo teorije razširjanja prostora (CET) za kompleksno analizo pilotov DDS. Ta metoda omogoča upoštevanje vpliva tehnologije pri načrtovanju pilotov. Predstavljen je splošen pregled CET ter opisani vsi koraki reševanja obravnavanega problema. Rezultate izračunov smo analizirali in primerjali z rezultati treh statičnih obremenilnih preizkusov. Analize vključujejo primerjavo krivulje obremenitev-pomik in porazdelitve obremenitve po dolžini pilota, ki je bila izmerjena z uporabo merilcev specifičnih deformacij. Rezultati analiz kažejo zelo dobro ujemanje izračunanih in izmerjenih vrednosti. Razlika med izračunanimi in izmerjenimi krivuljami obremenitev-pomik ni presegala 10 %. Predstavljene so tudi možnosti prihodnje uporabe CET.

1 INTRODUCTION

Piles are the most frequently used elements of deep foundations that are used to transfer a load from a structure to a suitable bearing stratum when the soil mass immediately below a construction is unsuitable for the direct bearing of footings. New technologies for the execution of pile foundations are constantly being developed due to the stricter requirements of modern structures. The most appropriate way of categorizing piles according to their technology is as large displacement, small displacement, and replacement piles [1]. This article focuses on Drilled Displacement System (DDS) piles. DDS technology is also known as DD (Drilled Displacement), FDP (Full Displacement Pile), or APGD (Auger Pressured Grouted Displacement) piles. DDS piles are rotary drilled piles with the full displacement of the soil in the horizontal direction, which leads to a higher bearing capacity of the pile in comparison with replacement piles (see for example [2, 3, 4]). Brown [5] published a general review of DDS technology and its advantages and disadvantages in comparison with other pile technologies.

In the past, several calculation methods for determining the ultimate resistance and load-settlement curve of the pile have been developed, for example [6, 7, 8, 9]. Zhang et al. [10] classified the calculations into five categories: simplified analytical methods, load-transfer curve methods, finite-element methods (FEMs), boundary-element methods (BEMs), and variation methods. The selection of the most appropriate method for a pile design depends on experience and availability, and plays a very important role in the accuracy of the solution. This article deals with the use of Cavity Expansion Theory (CET), published by Mecsi [11, 12], for an analysis of pile displacement. The CET theory seems to be one of the most appropriate methods for a given case, because the principles which are assumed, i.e., creating a cylindrical space (a pile body) and the horizontal displacement of the soil to the surrounding area, are very similar to the real installation process of a DDS pile. The method makes it possible to calculate the changes in soil properties that are affected by the cylindrical displacement of the soil and take them into account in the calculation.

It is difficult to summarize the results of all previous researchers, because the CET has been used for the design or analysis of many geotechnical constructions. An analysis using CET leads to useful solutions for a variety of problems in geotechnical engineering [11, 13, 14]. Examples of the applications are the bearing capacity of a displacement pile (or a partial displace-

ment pile) [15], interpretation of a pressure meter [11, 16, 17] and cone penetration tests (CPT), for example [18], and an analysis of the deformation around tunnels. The application of CET to many geotechnical solutions was published by Yu [19]. CET can be classified into a pressure-controlled cavity expansion and a displacement-controlled cavity expansion [20]. CET used for analytical solutions assumes various constitutive laws of the medium around the cavity, for example, linear elastic or elastic perfectly plastic, with or without accounting for the volume variation [21]. These theories were adopted for the soil behaviour under a small strain as well as a large strain [14, 22,]. With the advent of numerical modelling, various numerical models were used to analyse some of the problems of a cylindrical cavity for different tasks, for example [23]. Many published simulations, for example [13, 14, 24], assumed that the soil around the cavity is homogeneous and isotropic. Due to the change in the sedimentary environment and a consolidated environment, however, the initial stress in the soil layer is usually anisotropic [24]. The use of the axisymmetric CET to investigate the effect of soil parameters on the ground movement in the vicinity of static pipe-bursting operations was studied by Fernando and Moore [25]. They present a parametric study which shows that the ground movements are controlled by the soil strength and dilatancy, rather than by the elastic soil properties. The case studies prepared by Rao et al. [26] showed that it is necessary to consider the effect of the coefficient of horizontal earth pressure K_0 . Analytical solutions based on $K_0 = 1$ overestimate the critical expansion pressure and the ultimate expansion pressure as well as the plastic zone around the cavity. Li et al. [27] presented a solution that investigates the effect of the initial stress anisotropy and the initial stress-induced anisotropy on the cavity expansion by adopting parametric studies with different over-consolidation ratios (OCRs).

The results of fully instrumented static load tests on DDS piles are analysed and compared with the results of calculations using the CET. The analysis includes a comparison of the load-settlement curves as well as a comparison of the measured and calculated load distributions over the pile's length measured using strain-gauges. Detailed analyses of three tested DDS piles are presented in the article.

2 METHODOLOGY OF THE PILE DESIGN USING THE CAVITY EXPANSION THEORY

General definitions of the soil stress deformations and volume changes in the soil as well as an examination of the cylindrical expansion for a given CET were

presented by Mecsi [11]. He showed that the volume changes occurring in the soil are attributed to the laws of the soil stress forming around a cylinder. The hardening of the soil and the impact of the soil mass around the cylinder on the stress-strain state are taken into account in the calculation.

The presented theory supposes an axisymmetric stress state in the normally consolidated soil with incompressible soil grains. The anisotropic stress-strain state is taken into account in the initial conditions. It means that the compressive stresses in the vertical direction and the earth pressure at rest in the horizontal direction of the soil are assumed. The zone, where the soil density increased due to a process of enforced expansion, is also taken into account. The basic characteristics of the calculation model used are:

- application of the Mohr-Coulomb (MC) conditions (plastic stress state),
- force equilibrium,
- nonlinear relationship between increasing soil stress and soil strain,
- assumption of the elastic behaviour for the decrease of the soil stress,
- changes in the soil density are obtained as a result of the strain in three mutually perpendicular directions (the 3D effect of the soil deformation is included).

In the initial stress state, the original geostatic stress in the vertical direction and the horizontal stress at rest

are considered. Because the soil volume is changed (compressed), the plastic stress state is reached according to the MC law. The soil volume continues to change (increase) after the plastic stress state has been reached.

The following effects are applied in the calculation model:

- In the area outside the zone of compaction (elastic zone):*
- a nonlinear relation between the radial deformations and stresses for the compaction, and a linear one for the expansion,
 - the soil density (volume) is not changed.

- At the border of the compaction zone:*
- the same effects are applied as for the outside zone with some supplements,
 - the MC relation comes into effect.

- Within the plastic stress state zone (a zone of the compaction):*
- the MC relation is applied,
 - a nonlinear relationship between the radial deformations and the stresses for the compaction and a linear one for the expansion.

Individual assumptions and the steps of the calculations are simply described for the presented analyses, due to the extensiveness of the theory used. The basic assumption of the presented theory is shown in Fig. 1.

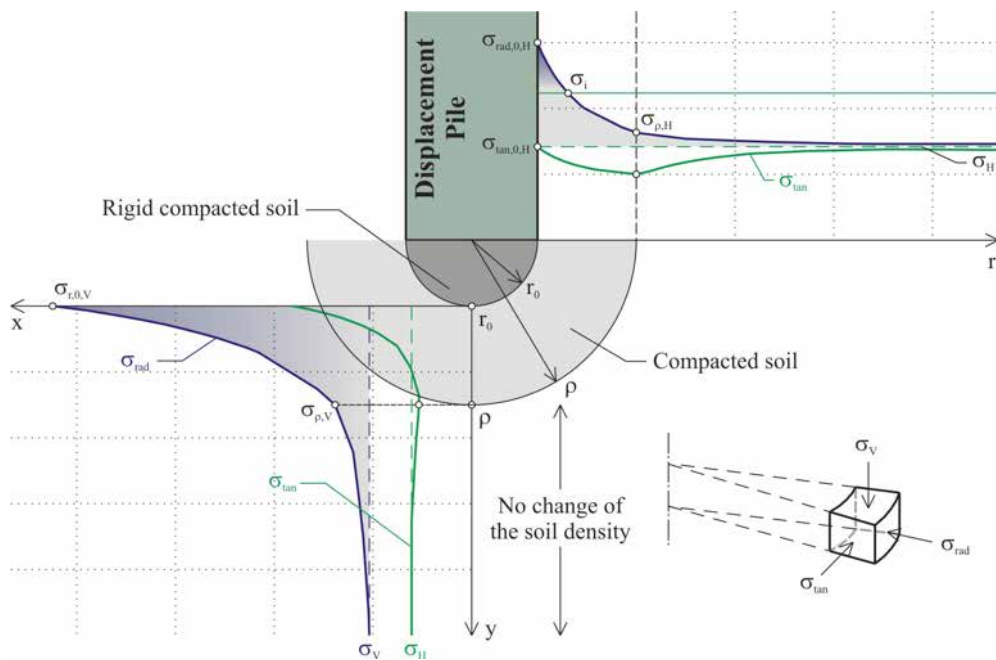


Figure 1. Description of the soil stresses near the bottom of the pile according to [11].

The distribution of the soil stresses acting beneath the pile bottom varies in the different directions. The soil immediately below the pile base becomes significantly harder after loading and a zone called the "rigid compacted soil" is created. The theory presented assumes that this fully compacted zone directly transfers a compressive load to the surrounding soil below the pile base. The radius of the fully compacted zone (rigid compacted soil) is equal to the pile radius r in the calculations. Based on this supposition, the base area of the pile in equation (5) is simply assumed to be πr^2 . When the load is applied to the pile, a spherical compacted zone is created from the bottom of the pile with the radius (ρ). In the first step of the calculations it is necessary to calculate the soil stresses at the boundary of the compacted zone ($\sigma_{r,V}$ in the vertical and $\sigma_{r,H}$ in the horizontal directions) with respect to the initial soil stresses (σ_V in the vertical and σ_H in the horizontal directions) using equations (1) and (2). The derivation process of both equations was described by Mecsi [11] in a step-by-step fashion.

$$m_r = 0 \Rightarrow \frac{\sigma_{\rho,V}^{(1-a)} - \sigma_V^{(1-a)}}{(1-a) \cdot E_0} - 2 \cdot \frac{\sigma_H - \xi \cdot (\sigma_{\rho,H} - \sigma_u)}{\sigma_H^a \cdot E_0} \Rightarrow \sigma_{\rho,V} \quad (1)$$

$$m_t = 0 \Rightarrow \frac{\sigma_{\rho,H}^{(1-a)} - \sigma_H^{(1-a)}}{(1-a) \cdot E_0} - \frac{\sigma_H - \xi \cdot (\sigma_{\rho,H} - \sigma_u)}{\sigma_H^a \cdot E_0} \Rightarrow \sigma_{\rho,H} \quad (2)$$

where m_r is the change in the volume in the radial direction, and m_t is the change in the volume in the tangential direction; σ_u is the unconfined soil strength; E_0 is the modulus of elasticity; and a is a parameter of the nonlinearity described below. This makes it possible to calculate the radius of the compaction zone ρ (extended plastic stress state), where the ultimate stress $\sigma_{r,H,limit}$ is also taken into account.

$$\rho = r_0 \cdot \left(\frac{\sigma_{r,H,limit} + \frac{c'}{\tan \varphi'}}{\sigma_{\rho,H} + \frac{c'}{\tan \varphi'}} \right)^{\frac{1+\sin \varphi'}{2 \cdot \sin \varphi'}} \quad (3)$$

The definition of the nonlinear deformation of the soil is one of the important points of the calculation. The effect of soil compaction is determined by changing the secant modulus using the parameter a . The parameter a can be determined according the results of an oedometer test. The secant modulus, which depends on the geostatic stress, is given by equation:

$$E_S = E_0 \cdot \left(\frac{\sigma}{\sigma_{ref}} \right)^a \quad (4)$$

The size of the vertical limit stress for the calculation of the ultimate pile base resistance $Q_{b,ultimate}$ is given by the difference between the vertical stress at the bottom of the pile under the load $\sigma_{r,0,V}$ and the initial geostatic stress σ_V . The value of $\sigma_{r,0,V}$ is given by equation (5). It is recom-

mended that the calculation be divided into more loading steps (from interval 0 to $Q_{b,ultimate}$) for the calculation of the load-settlement distribution under the pile base.

$$\sigma_{r,0,V} = \sigma_V + \frac{Q_b}{\pi \cdot r^2} \quad (5)$$

The distributions of the radial soil stress (σ_{rad}) and the tangential soil stress (σ_{tan}) as well as the distribution of the soil displacement ($\Sigma \Delta u_{r,i}$) allow a determination of the base resistance-soil displacement (compaction) curve. The distribution of soil stresses within the compacted (plastic) zone is statically determined under the force equilibrium and the Mohr-Coulomb conditions. The derivation process of the final equations presented was described in detail by Mecsi [11]. The radial soil stress distribution is given by the following equations:

- Inside the zone of compaction (if $r \leq \rho$):

$$\sigma_{r,V} = \left(\sigma_{\rho,V} + \frac{c'}{\tan \varphi'} \right) \cdot \left(\frac{\rho}{r} \right)^{\frac{4 \cdot \sin \varphi'}{1 + \sin \varphi'}} - \frac{c'}{\tan \varphi'} + \sigma_w \quad (6)$$

- Outside the zone of compaction (if $r > \rho$):

$$\sigma_{r,V} = (\sigma_{\rho,V} - \sigma_V) \cdot \left(\frac{\rho}{r} \right)^3 + \sigma_V \quad (7)$$

where σ_w represents the pressure of the water in the pores.

The change of the strain (in compression) is given by the equation:

$$\Delta \varepsilon_r = \frac{\sigma_{r,V}^{(1-a)} - \sigma_V^{(1-a)}}{(1-a) \cdot E_0} \quad (8)$$

and the change of the radial soil displacement is equal to:

$$\Delta u_{r,i} = \frac{\Delta \varepsilon_{r,i-1} + \Delta \varepsilon_{r,i}}{2} \cdot (r_i - r_{i-1}) \quad (9)$$

The shaft resistance and finally the load-settlement curve of the pile can be subsequently calculated after all the previous steps. The ultimate stress in the horizontal direction for the calculation of the ultimate shaft resistance is equal to:

$$\sigma_{r,H,limit} = \frac{\kappa \cdot \sigma_H}{\xi} + \frac{2 \cdot c'}{\sqrt{\xi}} \quad (10)$$

where κ is a multiple factor for the impact of the technology. Based on the Mohr-Coulomb relationship, the ratio of the principal stresses ξ can be expressed with the following correlation:

$$\xi = \frac{1 - \sin \varphi'}{1 + \sin \varphi'} \quad (11)$$

The ultimate shaft resistance of the pile is given by the ultimate shear strength along the pile using Coulomb's relationship:

$$\tau_{ult} = \sigma_{r,H,limit} \cdot \tan \varphi' + c' \quad (12)$$

and the shear resistance is given by the following equation:

$$t_{ult} = U_z \cdot \tau_{ult} \quad (13)$$

where U_z is the diameter of the pile at a depth z from the top of the pile.

Generally, the shear resistance is given by the equation:

$$t = \frac{u_{b+s}}{\Delta_M} \cdot t_{ult} \quad (14)$$

Elastic behaviour is considered up to the displacement Δ_M , which is required for the full mobilization of the shaft friction and u_{b+s} is the sum of the deformation of

the pile base and the pile shaft (settlement of the soil below the pile base and the axial compression of the pile body). When the value of Δ_M is reached, the plastic stresses are taken into account.

3 GEOLOGICAL CONDITIONS OF THE TESTED AREA

The geological conditions of the tested area consist of very soft layers with a thickness of about 13-15 m and very dense coarse-grained soils below them. The geologi-

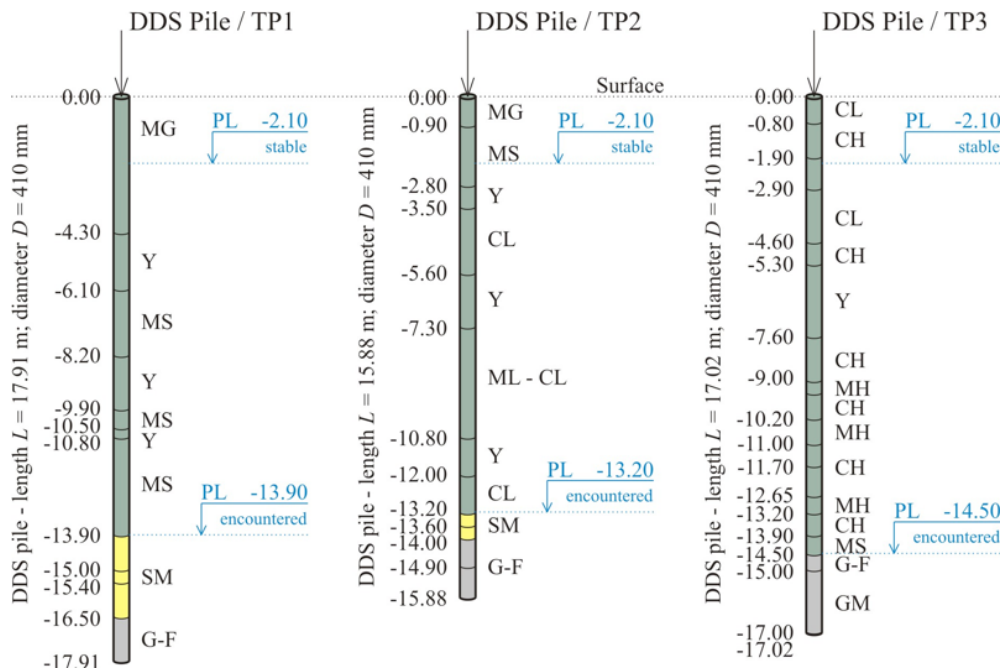


Figure 2. Geotechnical models of the analysed piles.

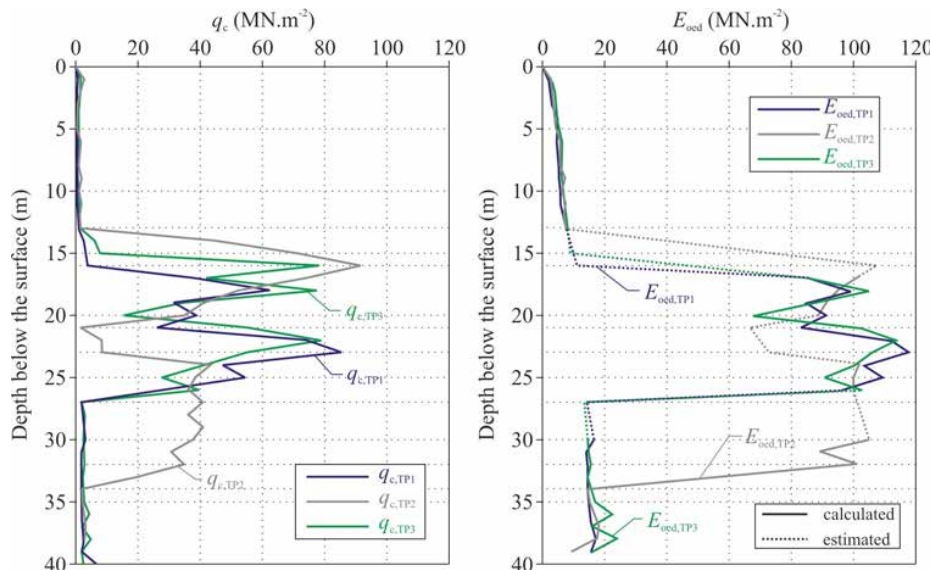


Figure 3. Results of CPT tests in the tested area.

Table 1. Soil properties used in the calculation.

Test pile	TP1			TP2			TP3	
	F	S	G	F	S	G	F	G
Symbol of soil	F	S	G	F	S	G	F	G
Depth (m)	-	13.90	16.50	-	13.20	14.00	-	14.50
Thickness (m)	13.90	2.60	1.41	13.20	0.80	1.88	14.50	2.52
γ (kN.m ⁻³)	19	18	19	19	18	19	19	19
γ_{sat} (kN.m ⁻³)	20	20	21	20	20	21	20	21
ϕ' (°)	20	28	37.5	20	28	37.5	20	37.5
c' (kN.m ⁻²)	20	10	1	20	10	1	20	0
E_s (kN.m ⁻²)	5160	28140	112000	6990	28140	117600	6600	119900
a (-)	0.5	0.4	0.1	0.5	0.4	0.3	0.5	0.3

cal profiles for the tested piles are shown in Fig. 2. The stratum of soft soil (0.00 to 13.20~14.50) is especially represented by sandy silts (MS), stiff silts, clays with low plasticity (ML-CL), and layers of organic clays (Y). In the case of TP3, soft soils were classified as clays with high plasticity (CH) and silts with high plasticity (MH). In the cases of TP1 and TP2, coarse-grained soils consist of silty sands (SM) of a thickness of 2.6 m (TP1) and 0.8 m (TP2). Very dense gravels with fine soils (G-F) are located below the sandy layers. In the case of TP3, coarse-grained soils consist of gravels with fine soils (G-F) and silty gravels (GM) immediately below the soft stratum.

An engineering-geological survey that was executed on the area of the tested piles included many in-situ tests and also standard laboratory tests [28]. The following were executed: 48 SPT tests, 54 CPT tests, 17 DPH tests, 10 piezometers and core drillings. The distributions of q_c and E_{oed} obtained using the correlation from the CPT test in the area of the tested piles are shown in Fig. 3. The soil properties used in the calculation are shown in Table 1.

Based on the results of the in-situ tests, the soft layers (0 to 13.20~14.50) have about the same mechanical soil properties. For this reason, the soft stratum is considered as homogeneous (separately in all profiles). The layer is marked using the symbol F (Table 1). The effective shear strength parameters ϕ' and c' were taken into account according to the results from the test report [28]. The impact of the groundwater was taken into account as a phreatic level under the pressure. The pore pressure was estimated as the difference between the encountered and the stable groundwater level (for example, TP2: (13.20 m to 2.10 m) * 10 kN.m⁻³ = 111 kN.m⁻²).

4 EXECUTION OF THE STATIC LOAD TEST

A static load test (SLT) is the most accurate method for pile design [7]. The fully instrumented SLT makes it

possible to obtain a complex overview of the interaction between the pile and the soils. The tested piles (TPs) were about 15 to 18 m long with a diameter of 410 mm. TP1 is 17.91 m long and anchored over 4.01 m into coarse-grained soils; TP2 is 15.88 m long and anchored over 2.68 m into coarse-grained soils; TP3 is 17.02 m long and is anchored over 2.52 m (Fig. 2). The settlement of the pile head, the horizontal aberration, the uplift of the reaction piles, and the distribution of the load over the pile's length using strain-gauges were recorded during the SLT and this allowed for a detailed analysis of the DDS pile. The static load tests were executed in 333-kN steps up to a maximum load of 2000 kN, including the unloading steps. As an example of the execution of the SLT of TP2: in the first phase of the SLT, the vertical load reached 1333 kN in four loading steps. After the unloading in the second step, the vertical load was increased to 2000 kN (in 333 kN steps) in the third phase. The unloading to 0 kN was carried out in the last

**Figure 4.** Details of the set up for the sensors in the static load test.

phase. The details of the set up for the sensors in the static load test are shown in Fig. 4.

5 COMPARISON OF THE RESULTS CALCULATED USING THE CET WITH THE RESULTS OBTAINED BY THE SLT

The load-settlement curves and the load distributions over the pile's length, which are calculated using the CET, are compared and analysed with the results of measurements obtained from the SLT. The analysis of the load-settlement curve and the load distribution over the pile's length plays a significant role and confirms the correctness of the calculation, because an analysis of only load-settlement curves could lead to a mistake in the evaluation of the pile resistance, as has been presented by, for example, Tosinini et al. [29]. The analysis of TP2 is presented in detail, step by step, according to the previous description of the calculation methodology.

Initially, the calculations of the pile-base resistance as well as the displacement below the pile base are presented. The increase in the radial stress $\sigma_{rad,i}$ in comparison with the geostatic stress $\sigma_{V,i}$ under the pile base is presented in Fig. 5. The values of $\sigma_{rad,i}$ are shown from a depth of $z = 0.205$ m, which is a rigid compaction of the soil, and is equal to the radius of the pile. The distributions of the tangential soil stress under the pile base $\sigma_{tan,i}$, compared with the horizontal geostatic stress at the rest $\sigma_{H,i}$ are also shown in Fig. 5.

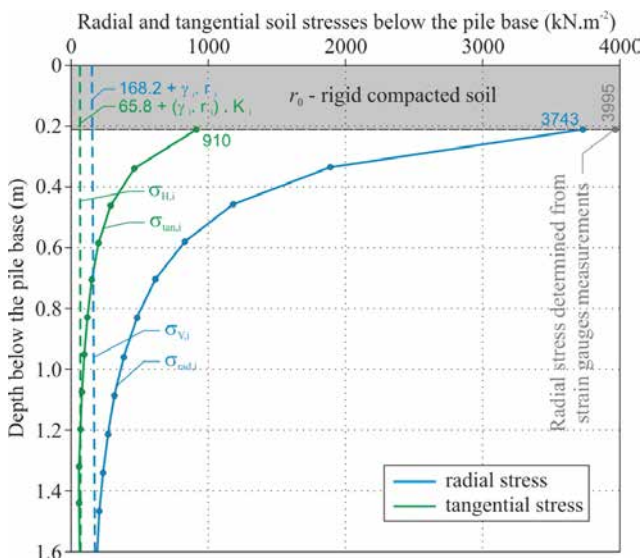


Figure 5. Distribution of the radial and tangential soil stresses below the pile base - TP2.

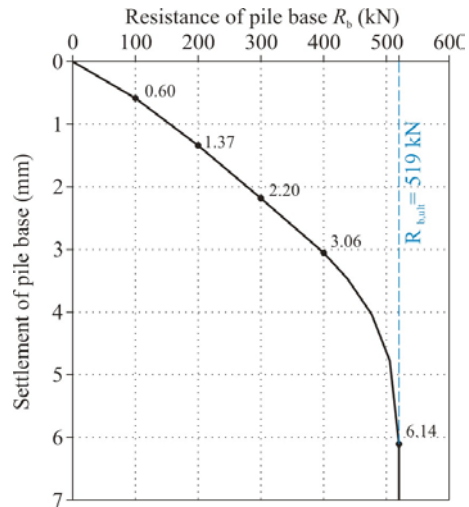


Figure 6. Resistance of the pile base-settlement curve - TP2.

The results presented are shown only for the magnitude of the vertical ultimate resistance of the pile base $Q_{b,ultimate}$, which is equal to the value of 519 kN. The resistance of the pile base depending on the soil displacement (compaction) is shown in Fig. 6.

In the next steps the ultimate stress $\sigma_{r,H,limit}$ and the ultimate shaft resistance, τ_{ult} and t_{ult} , are determined using equations (10), (12), and (13). The deformations required for full mobilization of the shaft friction Δ_M play a significant role in the calculation of the shaft resistance. The value of Δ_M was equal to 1.0 mm for

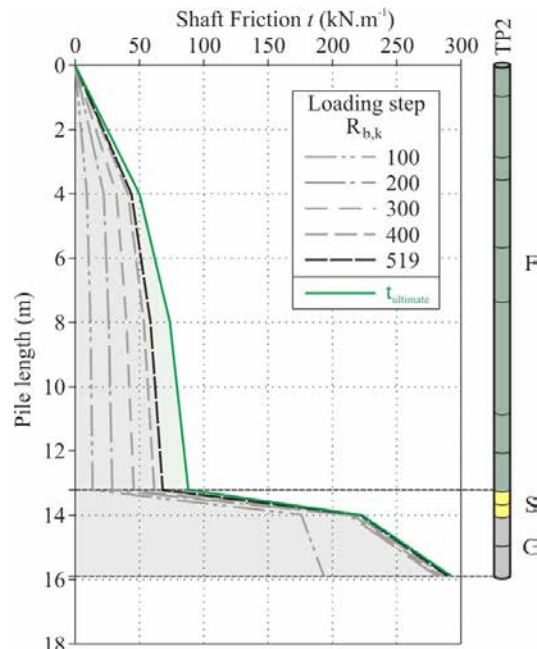


Figure 7. Distribution of the shaft friction over the pile length - TP2.

the coarse-grained soils and 10 to 20 mm for the fine-grained soils. The multiple factor κ was calculated according to the formulas for the displacement piles [11]. The distribution of the shaft friction over the pile's length is shown in Fig. 7. The presented curves are determined according to the results of the pile base (in the range from 0 to $R_{b,ult}$). The ultimate shaft friction t_{ult} is equal to the full mobilization of the shaft resistance (ultimate stress is moving in the plastic stress state).

These results make it possible to obtain a load distribution over the pile's length, as shown in Fig. 8. The calculated distribution of the load over the pile's length is compared with the measurements obtained using strain gauges in the static load test. This comparison confirms the correctness of the calculations. The difference between the calculated base resistance (519 kN) and the measured one (554 kN - SLT) is a 6% degree of accuracy. The difference at the boundary between the soft stratum and the coarse-grained soils (13.2 m) is a 4% degree of accuracy.

The comparison of the load-settlement curves obtained by the static load test and calculated using the CET is shown in Fig. 9. The comparison also includes the ratio of the pile base resistance to the total pile resistance. The results of the calculations are in good agreement with the measurements. The difference between the calculations and the measurements is less than about a 10% degree of accuracy.

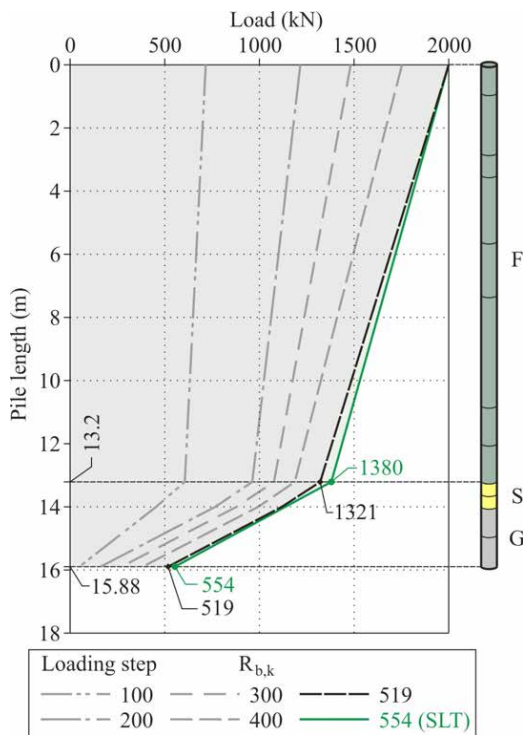


Figure 8. Distribution of the load over the pile's length - TP2.

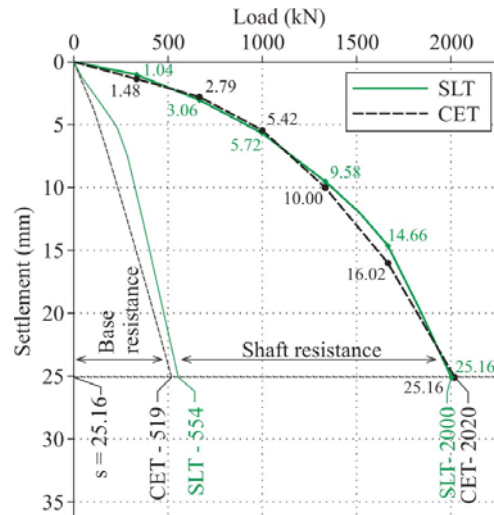


Figure 9. Load-settlement curve of DDS pile - TP2.

The results of the analyses of TP1 and TP3 are presented in the following part. The comparison of the calculated and measured load distributions over the pile's length (TP1) is shown in Fig. 10, and the comparison of the load-settlement curves is shown in Fig. 11.

As can be seen in Fig. 10, the calculated load distribution over the pile's length again provides a sufficient reliability. The difference between the calculated and measured load-settlement curves is less than a 5% degree of

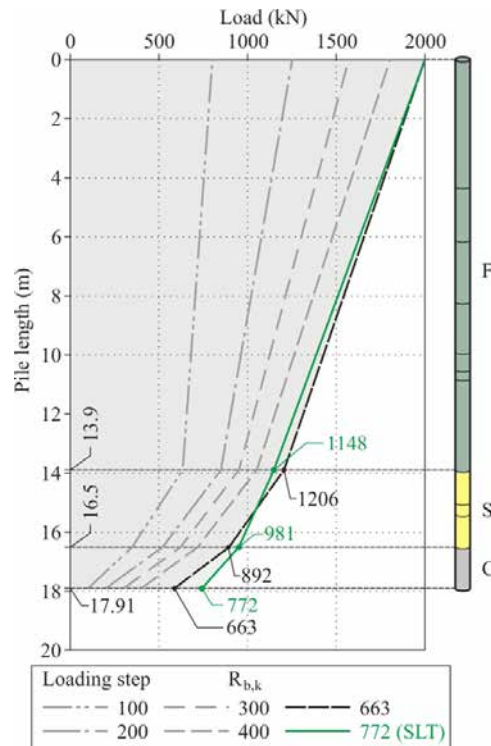


Figure 10. Distribution of the load over the pile's length - TP1.

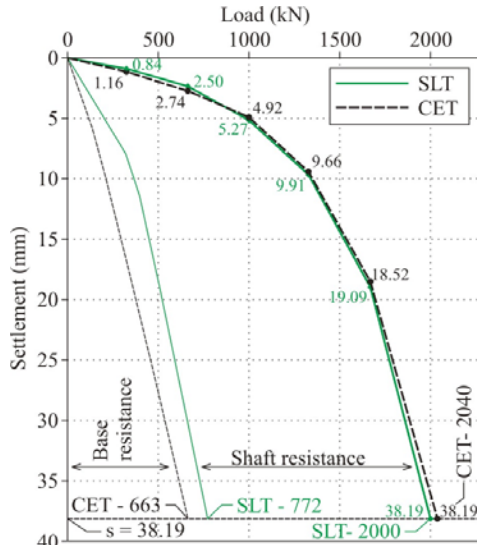


Figure 11. Load-settlement curve of DDS pile - TP1.

accuracy. A lower accuracy (< 15 %) is obtained for the pile-base resistance. It could be caused by insufficiently precise soil-strength parameters for the calculation of the pile base in this case, but the results are considered to be good enough. The results of the analyses of TP3 are presented in Fig. 12 and Fig. 13. Coarse-grained soils in the tested area of TP3 consist only of very dense gravels without any sand or sandy layers (Fig. 2), which leads to a higher bearing capacity.

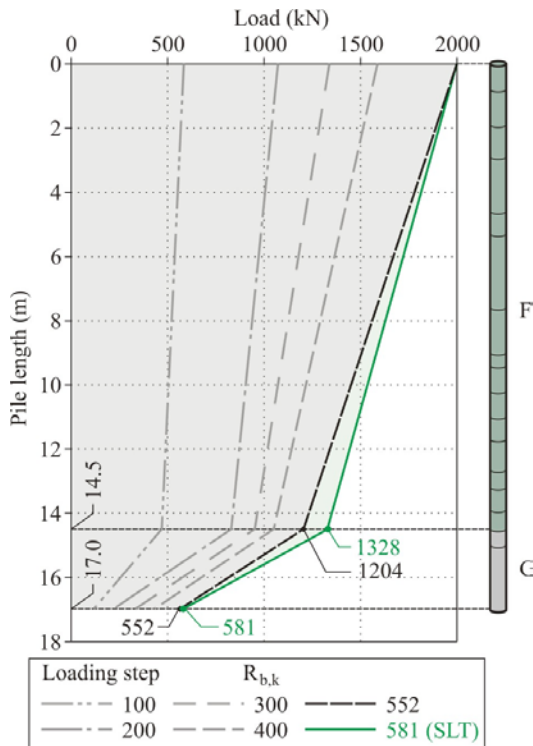


Figure 12. Distribution of the load over the pile's length - TP3.

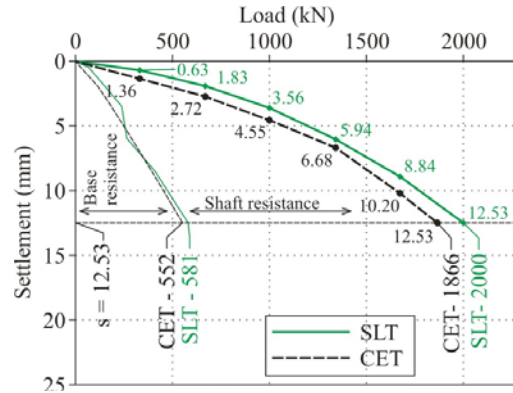


Figure 13. Load-settlement curve of DDS pile - TP3.

The vertical settlement of TP3 was significantly less than the previous ones. The use of the CET also allowed reliable results to be obtained in this case (TP3), while other methods (FEM and the Limit Load Curve Method according to Masopust [7]) were insufficiently accurate to reflect this difference [30].

In addition, CET makes it possible to calculate the changes of the stress state, the displacements, and the compaction around the pile that are affected by the pile technology. There are two different options for determining the pile resistance for a verification of the Ultimate Limit State (ULS). The first one is a determination of the pile resistance from a calculated load-settlement curve for a settlement equal to 10% of the pile diameter (41 mm in this case). The second one is the application of the presented theory in analytical calculation models. It is recommended that the characteristic values of the shaft resistance of the DDS pile can be calculated according to equation (15), taking into account the methodology presented.

$$R_{s,k} = \pi \cdot D \cdot \sum_{i=1}^n h_i \cdot (K_{H,i} \cdot \sigma_{or,i} \cdot \tan \varphi'_d + c'_d) \quad (15)$$

where $K_{H,i}$ is the coefficient of the horizontal earth pressure, which takes into account the impact of the technology; $\sigma_{or,i}$ is the geostatic stress at the middle of the i -layer; and φ'_d and c'_d are the effective parameters of the shear strength of the soil. Based on the CET method presented, the coefficient $K_{H,i}$ can be calculated using the following equation:

$$K_{H,i} = \frac{\sigma_{H,i} \cdot K_{\rho,H,i}}{\sigma_{V,i}} \quad (16)$$

where $\sigma_{V,i}$ is the vertical geostatic stress, $\sigma_{H,i}$ is the horizontal geostatic stress and $K_{\sigma,H,i}$ is the coefficient of the horizontal geostatic stress at the boundary of the compacted zone. This coefficient can be calculated using equation (2) or simply determined by using the diagrams presented by Mecsi [11].

6 CONCLUSION

Drilled Displacement System (DDS) piles are an innovative technology for pile foundations. DDS piles are created by rotary drilling, accompanied by a full horizontal displacement of the soil. The use of this technology can lead to a more effective and economical design in comparison with traditional pile technologies. Suitable geological conditions for DDS piles include sands, sandy gravels, and fine-grained soils, where a horizontal displacement can cause compaction of the surrounding soil. This process leads to an increase in the pile shaft's resistance.

The results of the three static load tests of the DDS piles are presented and analysed. These analyses include comparisons of the calculated load-settlement curves and load distributions over the pile length with the results of the static load test. A simple description of the methodology of CET is presented in the analysis of the test pile TP2. The detailed calculations include the distribution of the radial and tangential soil stresses, which are reflected in the pile base resistance-settlement curve. The calculations of the pile shaft's resistance include a determination of the shaft friction, the load distribution over the pile's length, and the load-settlement curve of the DDS pile. The analysis also includes changes to the soil stress state and the soil properties around the pile, which are affected by the pile technology.

The results of the analysis show very good agreement between the measurements and the calculations. The maximum difference between the load-settlement curves obtained using CET and SLT is equal to about a 10% degree of accuracy. The comparisons of the calculated and measured load distributions over the pile length provide the required degree of accuracy and confirm the correctness of the calculation methodology. The analyses confirm the suitability of the CET for the design of displacement piles. The CET allows a calculation of the soil properties, which are directly affected by the impact of the technology. These soil properties make it possible to take into account the impact of the DDS technology in analytical solutions of the pile resistance and they could also be used for numerical modelling.

Acknowledgments

The paper is one of the outcomes of the Grant VEGA agency No. 1 /0882/16: Influence of boundary conditions to limit states of geotechnical structures.

REFERENCES

- [1] Tomlinson, M., Woodward, J. 2007. Pile design and construction practice. 5th ed., Taylor & Francis e-Library.
- [2] Viggiani, C., Mandolini, A., Russo, G. 2012. Piles and pile foundations. Taylor & Francis, UK.
- [3] NeSmith, W. 2002. Static capacity analysis of augered, pressure-injected displacement piles. Int. Deep Foundations Congress, Florida, USA, pp. 1174-1186.
- [4] Zhussupbekov, A.Z., Ashkey, Y., Bazilov, R., Bazarbaev, D., Alibekova, N., Zhussupbekov, A. 2012. Geotechnical problems of new capital Astana (Kazakhstan). <http://www.mygeoworld.com/File/10268/geotechnical-problems-of-new-capital-astana-kazakhstan/download>, 10.10. 2017
- [5] Brown, D.A. 2005. Practical consideration in the selection and use of continuous flight auger and drilled displacement piles. Proc. Advances in design and testing deep foundations, Texas, USA, pp. 251-261. DOI: 10.1061/40778(157)1
- [6] Coyle, H.M., Reese, L.C. 1996. Load transfer for axially loaded piles in clay. Soil Mechanics and Foundations Division 92, 2, 1-26.
- [7] Masopust, J. 1994. Bored piles. Čenek a Ježek s.r.o., Prague, Czech Republic, [in Czech].
- [8] Nejad, F.P., Jaksa, M.B., Kakhi, M., McCabe, B.A. 2009. Prediction of pile settlement using artificial neural networks based on standard penetration test data. Computers and Geotechnics 36, 1125-1133.
- [9] Wang, Z., Xie, X., Wang, J. 2012. A new nonlinear method for vertical settlement prediction of a single pile and pile groups in layered soils. Computers and Geotechnics 45, 118-126. DOI: 10.1016/j.compgeo.2012.05.011
- [10] Zhang, Q.Q., Zhang, Z.M., Hej, Y. 2010. A simplified approach for settlement analysis of single pile and pile groups considering interaction between identical piles in multilayered soils. Computers and Geotechnics 37, 7-8, 969-976. DOI: 10.1016/j.compgeo.2010.08.003
- [11] Mecsi, J. 2013. Geotechnical engineering examples and solutions using the cavity expansion theory. Geotechnical Society Hungary, Budapest, Hungary.
- [12] Mecsi, J. 1996. Stresses, displacements, volume changes around the expansion cylinder in the soil. Proc. 10th Eur. Conf. Soil Mechanics and Foundation Engineering. Rotterdam, The Netherlands, pp. 243-246.
- [13] Vesic, A.S. 1972. Expansion of cavities in infinite soil mass. Soil Mechanics and Foundations Division 98, 3, 265-290.

- [14] Carter, J.P., Booker, J.R., Yeung, S.K. 1986. Cavity expansion in cohesive frictional soil. *Geotechnique* 36, 3, 349-358. DOI: 10.1680/geot.1986.36.3.349
- [15] Yu, H.S., Carter, J.P. 2002. Rigorous similar solutions for cavity expansion in cohesive-frictional soils. *Int. Journal of Geomechanics* 2, 2, 233-258.
- [16] Ladányi, B. 1963. Evaluation of pressuremeter tests in granular soils. *Proc. 2nd Pan American Conf. on Soil Mechanics and Foundation Engineering, Brazil, Vol. 1*, pp. 3-20.
- [17] Ervin, M.C. 1983. In-situ testing for geotechnical investigations. A.A. Balkema.
- [18] Salgado, R., Prezzi, M. 2007. Computation of cavity expansion pressure and penetration resistance in sands. *Int. Journal of Geomechanics* 7, 4, 251-265. DOI: 10.1061/(ASCE)1532-3641(2007)7:4(251)
- [19] Yu, H.S. 2000. *Cavity expansion methods in geomechanics*, Kluwer Academic Publishers Dordrecht, The Netherlands. DOI: 10.1007/978-94-015-9596-4
- [20] Au, S.K.A., Yeung, A.T., Soga, K. 2006. Pressure-controlled cavity expansion in clay. *Canadian Geotechnical Journal* 43, 7, 714-725. DOI: 10.1139/t06-037
- [21] Frikha, W., Bouassida, M. 2013. Cylindrical cavity expansion in elastoplastic medium with a variable potential flow. *Int. Journal of Geomechanics* 13, 1, 9-15. DOI: 10.1061/(ASCE)GM.1943-5622.0000166
- [22] Chadwick, P. 1959. The quasi-static expansion of a spherical cavity in metal and ideal soil. *The Quarterly Journal of Mechanics and Applied Mathematics* 12, 1, 52-71. DOI: 10.1093/qjmam/12.1.52
- [23] Zhou, W.H., Yin, J.H. 2008. A simple math model for soil nail and soil interaction analysis. *Computer and Geotechnics* 35, 3, 479-488. DOI: 10.1016/j.compgeo.2007.07.001
- [24] Xiao, Z.R., Zhang, Z., Du, M.F. 2004. An elastoplastic closed-form approach of cavity expansion in saturated soil based on modified Cam clay model. *Rock and Soil Mechanics* 25, 9, 1373-1378 [in Chinese].
- [25] Fernando, V., Moore, I.D. 2002. Use of cavity expansion theory to predict ground displacement during pipe bursting. *Pipelines 2002 - Beneath Our Feet: Challenges and Solutions*, American Society of Civil Engineers, Ohio, USA. DOI: 10.1061/40641(2002)81
- [26] Rao, P., Cui, J., Li, J. 2014. The elastoplastic solutions of cylindrical cavity expansion considering the $K_0 \neq 1$. *Proc. Advances in Soil Dynamics and Foundations Engineering GSP 240, Geo-Shanghai 2014, Shanghai, China*; pp. 433-443. DOI: 10.1061/9780784413425.044
- [27] Li, J., Gong, W., Li, L., Liu, F. 2017. Drained elastoplastic solution for cylindrical cavity expansion in K_0 -consolidated anisotropic soil. *Journal of Engineering Mechanics* 143(11). DOI: 10.1061/(ASCE)EM.1943-7889.0001357
- [28] Stacho, J., Ladicsova, E. 2014. Numerical Analysis of Drilled Displacement System Piles. *Proc. SGEM 2014, GeoConference on Science and Technologies in Geology, Exploration and Mining, Sofia, Bulgaria*, pp. 665-672. DOI: <http://dx.doi.org/10.5593/SGEM2014/B12/S2.085>
- [29] Tosini, L., Cividini, A., Gioda, G. 2010. A numerical interpretation of load tests on bored piles. *Computers and Geotechnics* 37, 3, 425-431. DOI: 10.1016/j.compgeo.2010.01.001
- [30] Stacho, J. 2013. Calculation of drilled displacement pile resistance by finite element method. *Proc. Advances in Architectural, Civil and Environmental Engineering, 23rd Annual PhD Student Conf., Bratislava, Slovakia*, pp. 498-505 [in Slovak].